NJC

Accepted Manuscript

This is an *Accepted Manuscript*, which has been through the Royal Society of Chemistry peer review process and has been accepted for publication.

Accepted Manuscripts are published online shortly after acceptance, before technical editing, formatting and proof reading. Using this free service, authors can make their results available to the community, in citable form, before we publish the edited article. We will replace this *Accepted Manuscript* with the edited and formatted *Advance Article* as soon as it is available.

You can find more information about *Accepted Manuscripts* in the Information for Authors.

Please note that technical editing may introduce minor changes to the text and/or graphics, which may alter content. The journal's standard Terms & Conditions and the Ethical guidelines still apply. In no event shall the Royal Society of Chemistry be held responsible for any errors or omissions in this *Accepted Manuscript* or any consequences arising from the use of any information it contains.

ROYAL SOCIETY OF CHEMISTRY

www.rsc.org/njc

Facile synthesis of $MgFe_2O_4$/C composites as anode materials for lithium-ion batteries with excellent cycling and rate performance

Ningning Huo[a, b, c, 1], Yanhong Yin[a, b, c, 1, *], Wenfeng Liu[a, b, c], Jun Zhang[a, b, c], Yanmin Ding[a, b, c], Qiuxian Wang[a, b, c], Zhenpu Shi[a, b, c], Shuting Yang[a, b, c, *]

[a] National & Local Joint Engineering Laboratory for Motive Power and Key Materials

[b] School of Chemistry and Chemical Engineering, Henan Normal University, Xinxiang Henan 453007, P. R. China

[c] Collaborative Innovation Center of Henan Province for Motive Power and Key Materials, Henan Normal University, Xinxiang Henan 453007, P. R. China

Corresponding Author

[*]E-mail: shutingyang@foxmail.com. Tel: (+86)-373-3326439.

Fax: (+86)-373-3326439.

Electronic supplementary information (ESI) available: additional scheme illustrations.

ABSTRACT: $MgFe_2O_4$/C material is prepared by a sol–gel auto-combustion process followed by carbon coating with glucose as carbon source. The obtained $MgFe_2O_4$/C sample shows remarkably enhanced specific capacity and rate performance. A reversible capacity of about 1965 mAh g^{-1} after 100 cycles at 0.1 C (107.2 mA g^{-1}) is

obtained. Specifically, the $MgFe_2O_4$/C composite electrode delivers a reversible specific capacity of 500 mAh g^{-1} even at 10 C (10000 mA g^{-1}), indicating excellent rate capability of the $MgFe_2O_4$ electrode.

KEYWORDS: Metal oxides, Anode materials, Lithium-ion batteries, Coulombic efficiency

1. Introduction

Transition metal oxides (TMOs, here TM = Mn, Co, Fe, Ni, Cu, etc.) have attracted fascinating research interest these years due to their high specific capacity (600-1200 mAh g^{-1}) and safer nature. Fe-based oxides, especially ferrites MFe_2O_4 (M = Ni, Cu, Co, Zn) stand out from TMOs due to their low cost and environmental benignity [1-4]. But unfortunately, their large volume change during Li^+ insertion/extraction, agglomeration, and low electronic conductivity hinder their applications in LIBs [5-7]. Through synthesizing nano-sized particles or compositing with carbonaceous materials [8-10], the cycling and rate performance of TMOs have been improved to a large extent. Ju Zhicheng et al. [11] fabricated uniform $NiCo_2O_4$ micro-nanostructured materials. About 650 mAh g^{-1} was maintained at a current density of 100 mA g^{-1} after 150 cycles. Moreover, it also exhibits an excellent rate performance, and delivers a stable reversible specific capacity of 450 mAh g^{-1} even at 2000 mA g^{-1}. Ju Zhicheng et al. [12] also prepared monodisperse $FeMoO_4$ nanocubes. It exhibits high reversible capacities of 926 mAh g^{-1} after 80 cycles at a current density of 100 mA g^{-1} and remarkable rate performance.

The spinel structure composite transition metal oxides $MgFe_2O_4$ is widely used as magnetic materials [13], catalyst [14] and humidity sensor [15]. Very recently, it is found $MgFe_2O_4$ can be used as anode material in lithium-ion battery. In the existing literature, $MgFe_2O_4$ shows relatively high initial capacity. But there is still a big gap with its theoretical value (1072 mAh g^{-1}). And its rate performance and cycling stability are relatively poor [6, 7, 16-18].

Two ways have been adopted to overcome these problems: one is to fabricate nano-sized $MgFe_2O_4$ [6, 16, 17], and the other is to combine $MgFe_2O_4$ with carbonaceous materials [7, 18-22]. Carbon coating has been proved to be an effective method to relieve the volume change and improve the electronic conductivity of TMOs [23]. However, only a few efforts have so far been dedicated to synthesizing $MgFe_2O_4$ and carbonaceous materials composites up to now. For example, Chen Gong et al. [7] prepared carbon-coated $MgFe_2O_4$ through co-precipitation method followed by subsequently heating with pyrrole in sealed autoclaves at 550 °C for 5 h. Alok Kumar Rai et al. [18] presented a urea-assisted auto-combustion method for synthesizing $MgFe_2O_4$/graphene nanocomposite. In these works, the highest stabilized specific capacity is less than 800 mAh g^{-1}. The cycling number is less than 150, and the highest current density used is 4.2 C.

So works should be done to improve its performance further. In addition, methods used and the synthetic procedure in the above works are relatively complicated. The process of the product costs much time. Some raw material is toxic and costly, which is unsuitable for large scale production. Moreover, the electrochemical performance is

not good.

Herein, we reported a facile approach for the synthesis of $MgFe_2O_4$/C using $Fe(NO_3)_3$• $9H_2O$, $Mg(NO_3)_2$• $6H_2O$ and citric acid as raw materials, followed by carbon coating with glucose as carbon source. Its cycling and rate performances were characterized. As a result, carbon coating by a facile method can not only improve the electrical conductivity of $MgFe_2O_4$, but also inhibit its growth of the particles, which can effectively shorten the lithium ion diffusion pathway.

2. Experimental

All chemicals used in this work are of analytical reagent grade, commercially available and without further purification.

2.1. Material Preparation

$MgFe_2O_4$ nanoparticles denoted as MFO were synthesized by a sol-gel auto-combustion process. In a typical synthesis of MFO, 0.02 mol $Mg(NO_3)_2$• $6H_2O$, 0.04 mol $Fe(NO_3)_3$• $9H_2O$ and 0.09 mol citric acid were dissolved in 80 mL deionized water. Then about 30 mL ammonia water (25 wt%) was dripped into the mixture under continuous stirring until it transformed into celadon sol (whose pH value equals to 7.0). Then the resultant solution was heated at 65 °C until it turned into a transparent gel. The gel was dried at 120 °C and followed by being heated at 200 °C to incur the auto-combustion progress. Finally, the brown and fluffy dendritic precursor was calcined at 700 °C for 2 h in muffle furnace.

Carbon coating was performed by mixing the as-synthesized MFO with glucose solution (MFO:glucose=3.6:1, which was the mass ratio), followed by evaporating the

water. And then the mixture was calcined at 500 °C for 2 h in N_2 to get the MFO/C sample. The detailed synthetic procedure could be seen in the Scheme S1.

2.2. Material Characterization

Structure of the MFO and MFO/C was identified by x-ray diffraction (XRD, Bruker AXS D8) analysis with Cu Ka radiation. The morphology was conducted with a transmission electron microscopy (TEM, JEM-2100, JEOL) and field emission scan electron microscopy (FESEM). X-ray photoelectron spectroscopy measurements were performed with a Kratos Axis Ultra DLD using the mono Al Kα radiation (1486.6 eV). Chemical composition of the MFO/C was determined by energy dispersive spectroscopy (EDS). Carbon content (wt%) in the obtained samples was determined by thermogravimetric analysis (TGA; Shimadzu TGA-50) at a heating rate of 10 °C min^{-1} in air. Raman spectra (Renishaw Invia) were obtained using 514 nm Ar^+ laser excitation with a power of 8.5 mW. The spectra were recorded in wave number range between 2000 and 800 cm^{-1}. For electrochemical evaluation, the MFO/C and MFO working electrode were made by mixing the active material, conducting agent (Super P) and binder (polyvinylidene fluoride) with N-methyl-2-pyrrolidine (NMP) as solvent at the ratio of 40:40:20 (wt%), which has been optimized in our previous work [24]. The loading in each electrode was about 1.6 mg cm^{-2}. The separator was a polypropylene membrane with micropores (Celgard 2400). Lithium metal was used as counter and reference electrode. The electrolyte used was 1M $LiPF_6$ in a mixture of ethylene carbonate (EC) and diethyl carbonate (DEC) (1:1volume). Galvanostatic charge–discharge experiment data were collected using LAND Cell test system

(CT2001A, Wuhan, China). AC impedance was carried out using an electrochemical workstation (CHI660B, Shanghai, China). For the impedance measurements, a perturbation of 10 mV was applied and the frequency range applied is from 0.1 Hz to 100 kHz.

3. Results and discussion

In this paper, nano-sized $MgFe_2O_4$ was prepared using sol-gel auto-combustion method with lower melting point and low cost nitrate as raw material and citric acid as complexing agent. Then adopting the prepared $MgFe_2O_4$ as precursor, $MgFe_2O_4$/C composite was synthesized using glucose as carbon source. After carbon coating, the particle size decreases and its electrical conductivity is enhanced. The relatively smaller particles are beneficial for Li^+ diffusion. The conductive carbon layer on the surface of the particles can act as a buffering matrix to relax the expansion of the active material electrode during the lithiation/delithiation process and a barrier to suppress the aggregation of active particles.

3.1. Material Characterization

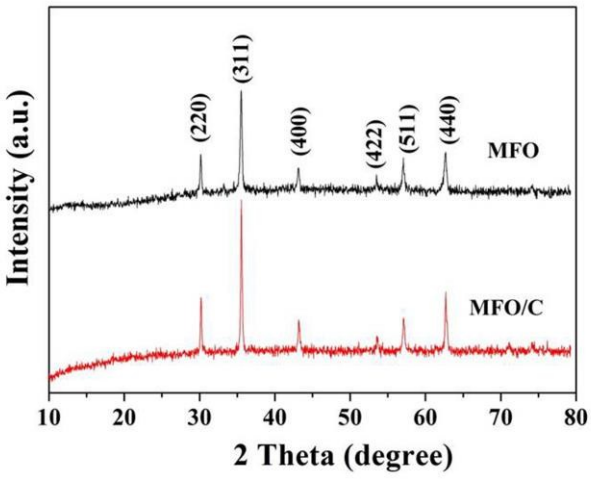

Fig. 1. XRD patterns of the MFO and MFO/C materials.

XRD patterns of the MFO and MFO/C are shown in Fig. 1. As can be seen, the two XRD patterns show no significant difference, which can be indexed to spinel MFO phase (JCPDS Card Files, No.17-0464, Fd-3m). No obvious impurity phase is detected. For MFO/C, no diffraction peaks for carbon are witnessed, suggesting that the carbon generated by decomposition of glucose may be amorphous.

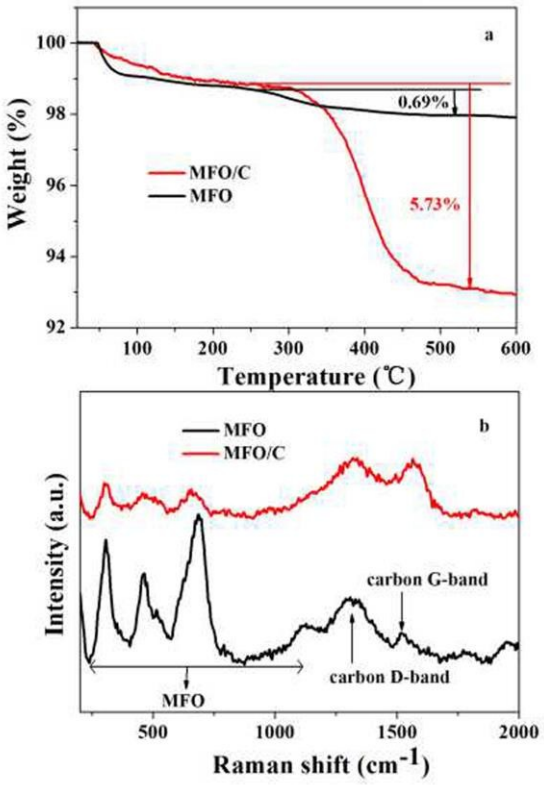

Fig. 2. TG analysis (a) and Raman spectra (b) of the MFO and MFO/C samples.

Fig. 2a is the TG curves of the MFO and MFO/C samples. As one can see, the weight loss before 250 °C is from the absorbed water. The weight loss during 250–600 °C can be attributed mostly to the removal of carbon in the samples [25, 26]. It seems that there exists about 0.69% carbon in MFO, which can be ascribed to the residual carbon coming from citric acid. The carbon content of the MFO/C composites is determined as 5.73%, most of which are from the decomposition of

glucose.

Raman measurements are employed to characterize the mode of occurrence of carbon in the samples. As shown in Fig. 2b, the band at 1311 cm^{-1} corresponds to the D band which is on behalf of degree of disorder, while the band at 1525 cm^{-1} is in good agreement with the G band which is characteristic for graphitization [9, 27-29]. The intensity ratio of the D and G band (I_D/I_G) is indicative of the degree of graphitization [30-32]. The ratio value for MFO is higher than that of MFO/C, implying that graphitization degree of carbon in MFO/C is higher than that in MFO. The higher content and graphitization degree of carbon in MFO/C are beneficial to the improvement of its electrical conductivity, and as a result, the electrochemical performance can be enhanced.

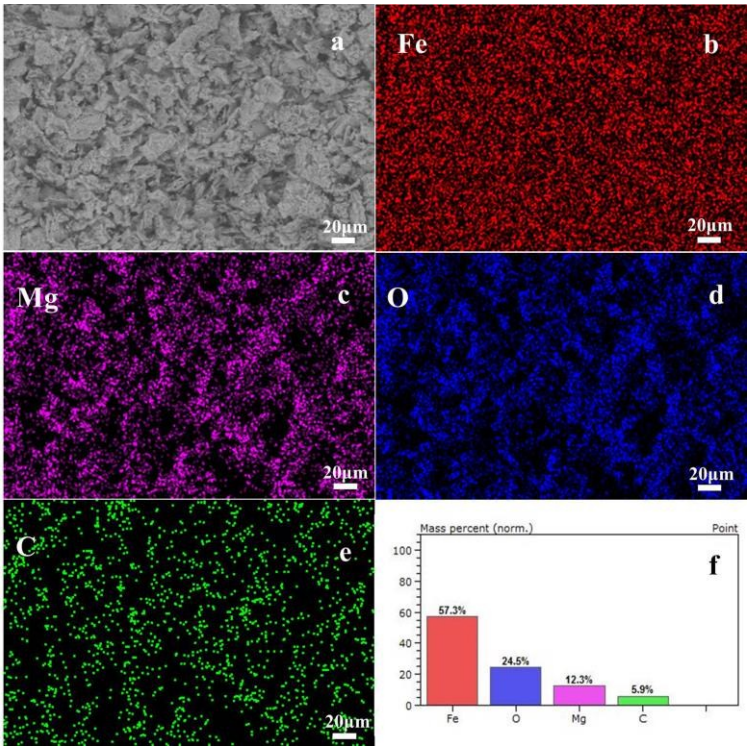

Fig. 3. Elemental mapping images of Fe (b), Mg (c), O (d) and C (e) and the histogram of atomic ratio (f).

Composition of the synthesized MFO/C is shown in the EDS spectra. As observed in Fig. 3b-e, the distribution of Fe, Mg, O and C in the sample is uniform. Fig. 4f reveals that the atomic ratio of Mg:Fe:O is approximately 1:2:4, which is consistent with the expected stoichiometry. The content of carbon is 5.9%, which is in accordance with the TG result.

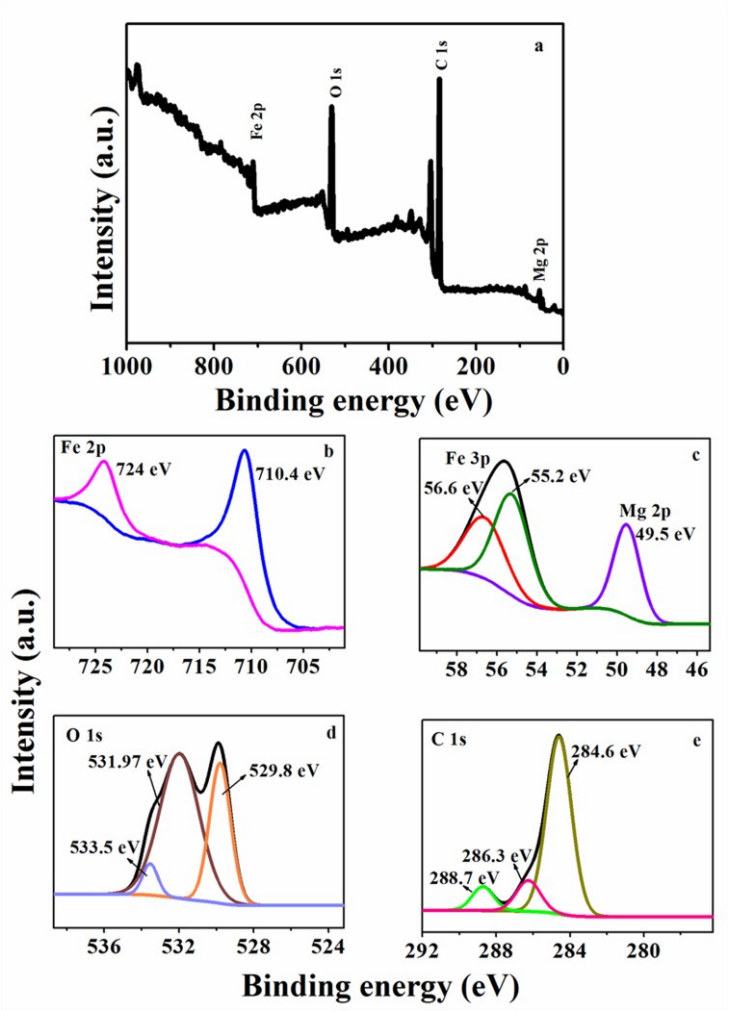

Fig. 4. X-ray photoelectron spectrum of MFO/C. (a) Overall XPS, (b) Fe 2p, (c) Mg 2p and Fe 3p, (d) O 1s and (e) C 1s.

The oxidation state of the constituent elements of MFO/C is determined by XPS in Fig. 4. Fig. 4a shows the overall XPS spectra, revealing the existence of Fe, Mg, O and C elements. Fig. 4b shows the Fe 2p spectrum. Two strong peaks located at 724.0

eV for Fe 2p1/2 and 710.4 eV for Fe 2p3/2 are detected, indicating the existence of Fe^{3+} in $MgFe_2O_4$ [10, 33, 34]. In addition, as shown in Fig. 4c, peaks located at 55.2 and 56.6 eV for Fe 3p demonstrate the existence of Fe^{3+} once again. As shown in Fig. 4c, the binding energy around 49.5 eV corresponds to Mg 2p, which is consistent with that reported for Mg^{2+} in the literature [35, 36]. Fig. 4d shows O 1s peaks. The peak at 529.8 eV can be assigned to O-Fe(Mg), while the rest two peaks at 532.0 and 533.5 eV can be attributed to the absorbed moisture in the sample [37] and the presence of residual oxygen-containing groups (such as OH and COOH) bonded with carbon atoms in the carbon layer of the MFO/C [30]. The deconvolution of C 1s spectrum (Fig. 4e) shows the presence of non-oxygenated carbon at 284.6 eV [10, 30, 38], C-O at 286.3 eV [6], and C=O at 288.7 eV [10, 38], which may come from the incomplete thermal decomposition product of citric acid and glucose.

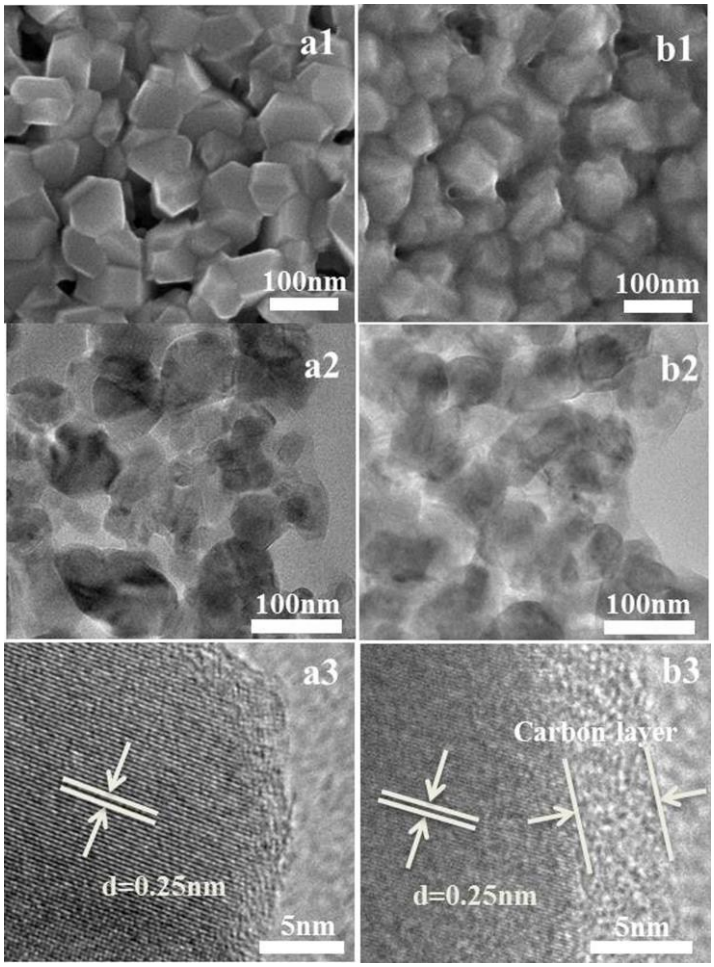

Fig. 5. FESEM, TEM and HRTEM images of MFO (a1, a2 and a3) and MFO/C (b1, b2 and b3).

Representative FESEM and TEM images of the MFO and MFO/C samples are given in Fig. 5. For the MFO sample (Fig. 5a1 and a2), the size of the particles is around 60 nm. When the MFO was coated with a carbon layer around 5 nm (Fig. 5b1 and b3), the morphology of the particle does not vary nearly (Fig. 5b1). Whereas, the particle size reduces slightly (Fig. 5b1), implying that carbon coating can affect the particles. Maybe gas produced from the decomposition of the hydrocarbon reduces the particle size. For the MFO sample, because the carbon content is so few that one

cannot find the carbon layer (Fig. 5a3). The distance between two neighboring fringes is 0.25 nm for MFO and MFO/C, corresponding to the lattice spacing of (311) plane.

3.2. Electrochemical Performance

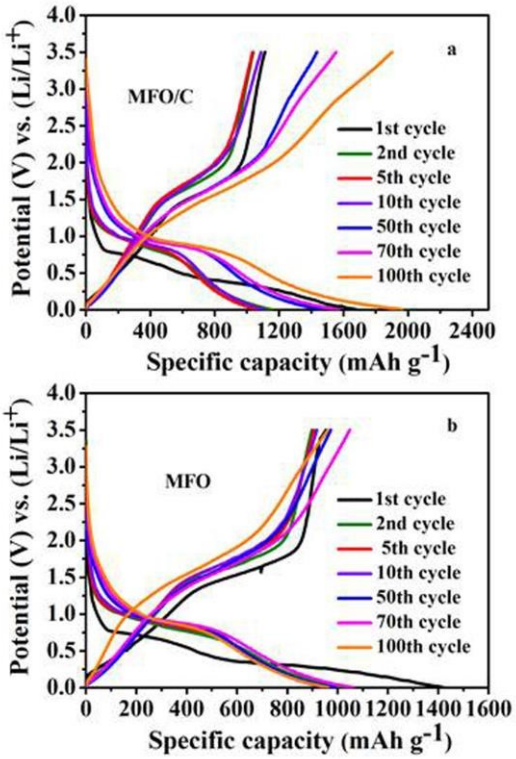

Fig. 6. Galvanostatic curves of the MFO/C (a) and MFO (b) electrode for the 1st, 2nd, 5th, 10th, 30th, 50th, 70th and 100th cycles at a current density of 107.2 mA g^{-1}.

Fig. 6(a, b) displays the discharge/charge voltage curves at a current density of 107.2 mA g^{-1} in a potential range of 0.005 - 3.5 V (vs. Li^+/Li). The capacity is calculated based on the mass of $MgFe_2O_4$/C. As observed for MFO/C in Fig. 6a, the initial discharge curve exhibits two plateaus at 0.4 and 0.78 V, respectively, which are associated with the irreversible and reversible reactions of MFO/C with Li^+. The first discharge capacity reaches as high as 1679.9 mAh g^{-1}. And the charge capacity is about 1112.5 mAh g^{-1} with the initial coulombic efficiency of 66.2%. The large capacity loss and low coulombic efficiency for the first cycle can be attributed to the

irreversibility of reaction and formation of SEI film [32]. From the second cycle, the charge/discharge specific capacity begins to decrease slowly until the 5th cycle. After that, the capacity slowly increases, which could be contributed to the interfacial lithium storage and/or reversible formation of polymeric/gel-like layer [39-41]. In contrast, for the bare MFO electrode (Fig. 6b), the initial discharge specific capacity reaches 1419.4 mAh g^{-1} with an initial coulombic efficiency of 67.4%. With cycling, one cannot observe the obvious capacity slowly rising phenomenon. As to the relatively lower coulombic efficiency of the MFO/C electrode, the reason maybe that the relatively smaller particle size and amorphous carbon coating will enlarge its specific surface, resulting in the increase of the irreversible formation of SEI film. But with cycling, the relatively larger specific surface may induce the capacity slowly rising phenomenon.

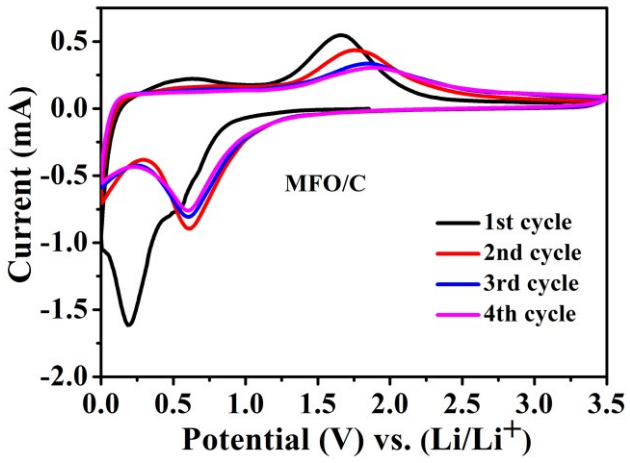

Fig. 7. The cyclic voltammogram of the MFO/C electrode at a scan rate of 0.25 mV s^{-1}.

Fig. 7 displays the cyclic voltammetry (CV) curve at scan rate of 0.25 mV s^{-1} in the voltage range of 0.0 - 3.5 V vs Li^+/Li. As seen in Fig. 7, in the first cycle, the

$MgFe_2O_4$/C shows a small peak at 0.53 V, which could be assigned to the formation of stable intermediate $Li_nMgFe_2O_4$. The following cathodic peak at 0.19 V could be ascribed to electrochemical reduction of Fe^{3+} to Fe^0, and the formation of Li_2O. The anodic peak located at 1.65 V could be attributed to the oxidation of Fe^0 to Fe^{3+}. In the subsequent cycles, cathodic peak shifts to more positive potential, which could be attributed to polarization of the electrode materials [11, 12, 18, 42]. Moreover, the CV curves are nearly superimposed after the first cycle, further demonstrating the excellent capacity retention of $MgFe_2O_4$/C electrodes.

According to the literature [42] and combined with the above analysis, the electrochemical reactions for the $MgFe_2O_4$/C electrode can be clarified as follows:

$$MgFe_2O_4 + nLi^+ + ne^- \rightarrow Li_nMgFe_2O_4 \quad (1)$$

$$Li_nMgFe_2O_4 + (6\text{-}n)Li^+ + (6\text{-}n)e^- \rightarrow 2Fe^0 + MgO + 3Li_2O \ (0 \leqslant n) \quad (2)$$

$$2Fe^0 + 3Li_2O \leftrightarrow Fe_2O_3 + 6Li^+ + 6e^- \quad (3)$$

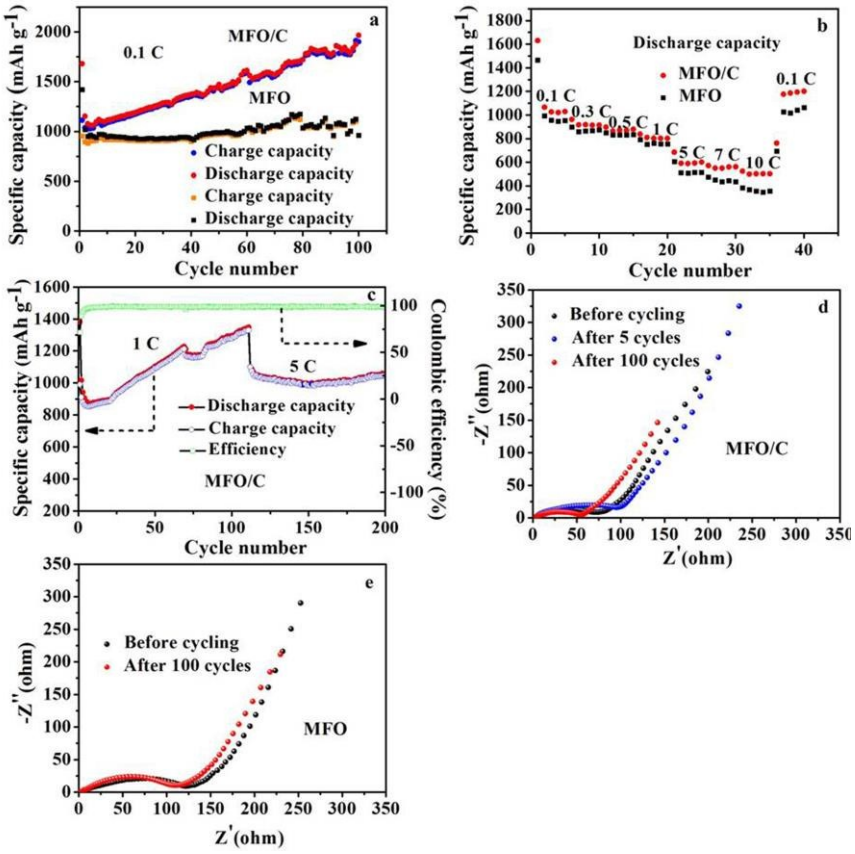

Fig. 8. (a) Cycling performance of the MFO and MFO/C electrode at 0.1 C (1 C = 1072 mA g^{-1}). (b) Cycling performance of the MFO and MFO/C electrode at 0.1 C, 0.3 C, 0.5 C, 1 C, 5 C, 7 C and 10 C (1 C = 1000 mA g^{-1}), respectively. (c) Cycling performance of the MFO/C electrode at 1 C and 5 C (1 C = 1000 mA g^{-1}). Nyquist plots of MFO/C (d) and MFO (e) electrode under full charged condition at 0.1 C (1 C = 1072 mA g^{-1}).

Cycling performances of the MFO and MFO/C electrode at different current rates are shown in Fig. 8a-c. In Fig. 8a, one can observe that the MFO/C electrode shows a high initial discharge capacity followed with gradual decrease until the 5th cycle, and then the capacity increases slowly. This capacity rising phenomenon has been widely reported for TMO electrodes, which can be ascribed to the reversible formation of polymeric/gel-like layer and/or interfacial lithium storage. On the basis of the related

literatures [39, 41, 43-46], this phenomenon can be reasonably explained by the following aspects. Firstly, the gradual formation of gel-like film resulting from the degradation of electrolyte on the surface of metal oxide, can prevent the aggregation of active materials and mitigate the volumetric variation upon cycling [44, 45]. Secondly, active materials coated by carbon layer may transform into smaller particles during cycling, which can increase the specific surface to some extent, thus leading to the enhancement of the interfacial Li storage ability and the increase of capacity [41]. Thirdly, the existence of Li_2O formed during the electrochemical process can not only effectively prevent the aggregation of active materials, leading to the retaining of the surface area, but also enhance the capacity related to the gel-like film [43]. Additionally, with the redox of Fe^{3+}, new interface produces constantly, leading to the capacity increases. Finally, the as-formed metal nanoparticles can catalyze the formation and dissolution of the electrolyte, enhancing the reversible ability of electrochemical reaction [44, 46].

The MFO/C electrode exhibits a high reversible capacity of about 1965 mAh g^{-1} after 100 cycles. This specific capacity is much higher than the theoretical specific capacity of $MgFe_2O_4$ (1072 mAh g^{-1}), which can be attributed to the reversible formation of polymeric/gel-like layer and/or interfacial lithium storage [47, 48]. During cycling, active materials may transform into smaller particles, which can increase the specific surface to some extent. Thus, more polymeric/gel-like layer and interface for Li storage can be formed, leading to the increase of capacity [41, 49]. In contrast, the MFO electrode shows stable capacity of around 980 mAh g^{-1}. The

reasons for the excellent cycling performance of the MFO/C electrode can be deduced as follows: one is that the conductive carbon layer on the surface of the particles can act as a buffering matrix to relax the expansion of the active material electrode during the lithiation/delithiation process and a barrier to suppress the aggregation of active particles. The other is that the existing carbon can decrease the particle size, which has been proved in Fig. 5. The relatively smaller particles are beneficial for Li^+ diffusion. In addition, carbon coating can effectively increase the electrical conductivity of the MFO particles. Therefore, the electrochemical performance and cycling stability will be enhanced. While for the MFO electrode, the carbon content is too few to play an effective role in improving its electrochemical performance.

In addition to the improved cycling performance, the MFO/C composite electrode also displays good rate performance. Fig. 8b is the rate capability at 0.1 C, 0.3 C, 0.5 C, 1 C, 5 C, 7 C and 10 C (1 C corresponding to 1000 mA g^{-1}), respectively. Specifically, the electrode delivers a reversible specific capacity of 500 mAh g^{-1} even at 10 C, indicating that MFO/C composites can tolerate high current charge/discharge cycling. When the current density is recovered to 0.1 C, a discharge capacity of as high as 1200 mAh g^{-1} is obtained. Compared with the MFO/C composite, rate performance of the bare MFO particles is inferior, especially at high current density. For example, when the current density is 10 C, capacity of the MFO electrode is only about 360 mAh g^{-1}. Cycling stability of the MFO/C electrode at 1 C and 5 C is shown in Fig. 8c. Capacity slowly rising phenomenon can also be found when the electrode is cycled at 1 C. At 5 C, the capacity could be sustained at about 1000 mAh g^{-1} after

200 cycles. In comparison with the recent reports on MFO anode materials, MFO/C composite shows outstanding rate capability and good cycle stability (Table 1).

Table 1 Electrochemical properties of MFO anode materials in literature in comparison to that in this work.

Anode materials	Specific capacity (mAh g^{-1})	Cycles	Rate capacity (mAh g^{-1})	the content of conducting agent	ref
$MgFe_2O_4$ nanoparticles	300	10		8:1:1	[17]
$MgFe_2O_4$ nanoparticles	493 at 90 mA g^{-1}	50	750 at 180 mA g^{-1}	7:2:1	[6]
$MgFe_2O_4$ nanoparticles	425 at 0.1 C (20 mA g^{-1})	40	290 at 0.5 C	80:12:8	[16]
$MgFe_2O_4$/C	744 at 100 mA g^{-1}	160	612.7 at 200 mA g^{-1}	8:1:1	[7]
$MgFe_2O_4$/grapheme	764.4 at 0.04 C (42.88 mA g^{-1})	60	219.9 at 4.2 C	7:2:1	[18]

Electrochemical impedance spectroscopy (EIS) of the MFO/C and MFO electrode under full charged condition is shown in Fig. 8d and e. According to Fig. 8a, difference between the capacities at the whole cycling process of the MFO electrode is relatively small, so only EIS before cycling and after 100 cycles was measured.

Nyquist plots of the MFO/C and MFO electrode show a similar shape, which consisted of a semicircle in the high frequency range and an inclined line in the low frequency range. The semicircle diameters in high frequency region is assigned to the charge transfer resistance (Rct), which is related to lithium ion interfacial transfer between the electrolyte and the active material. The inclined line in the low frequency region corresponds to the Warburg impedance, which is related to the solid-state diffusion of lithium-ion into the bulk of the active materials. One can notice that the value of the charge transfer resistance for the MFO/C electrode increases firstly and decreases after 5 cycles, which can shed light on the capacity rising phenomenon. But for the MFO electrode, the value varies little. In addition, the charge transfer resistance for the MFO/C electrode is lower than that for the bare MFO electrode. This indicates that the charge-transfer process of the MFO/C electrode is improved after the incorporation of carbon.

4. Conclusions

In summary, performance of the $MgFe_2O_4$/C (MFO/C) material prepared by a sol-gel auto-combustion process followed by carbon coating with glucose as carbon source has been reported. This material exhibits an outstanding electrochemical performance for Lithium-ion batteries in terms of superior cycling capability (1965 mAh g^{-1} after 100 cycles at 107.2 mA g^{-1}) and excellent rate performance (500 mAh g^{-1} at 10000 mA g^{-1}). The carbon coating is proved to be the key reason for the enhanced electrochemical behavior. Firstly, the existing carbon can decrease the particle size and increase the electrical conductivity of the MFO particles. Secondly,

carbon layer on the surface of the particles can act as a buffering matrix to relax the expansion of the active material electrode during the lithiation/delithiation process. This work shows that exploring carbon coating $MgFe_2O_4$ materials might open venues for the practical applications of TMO anodes in the next-generation of high-performance Li-ion batteries.

Acknowledgments

This work is financially supported by the National Natural Science Foundation of China under award NO. 21001041.

References

[1] M. Pileni, *Nat. Mater.*, 2003, **2**, 145-150.
[2] C. Burda, X. Chen, R. Narayanan, M. El-Sayed, *Chem. Rev.*, 2005, **105**, 1025-1102.
[3] P. Hu, L. Yu, A. Zuo, C. Guo, F. Yuan, *J. Phys. Chem. C*, 2009, **113**, 900-906.
[4] X. Guo, X. Lu, X. Fang, Y. Mao, Z. Wang, L. Chen, X. Xu, H. Yang, Y. Liu, *Electrochem. Commun.*, 2010, **12**, 847-850.
[5] Q. Hao, H. Ma, Z. Ju, G. Li, X. Li, L. Xu, Y. Qian, *Electrochim. Acta*, 2011, **56**, 9027-9031.
[6] Y. Pan, Y. Zhang, X. Wei, C. Yuan, J. Yin, D. Cao, G. Wang, *Electrochim. Acta*, 2013, **109**, 89-94.
[7] C. Gong, Y. Bai, Y. Qi, N. Lun, J. Feng, *Electrochim. Acta*, 2013, **90**, 119-127.
[8] L. Yao, X. Hou, S. Hu, J. Wang, M. Li, C. Su, M. Tade, Z. Shao, X. Liu, *J. Power Sources*, 2014, **258**, 305-313.
[9] Y. Qi, N. Du, H. Zhang, P. Wu, D. Yang, *J. Power Sources*, 2011, **196**, 10234-10239.
[10] J. Kim, Y. Kim, Y. Noh, W. Kim, *RSC Adv.*, 2014, **4**, 27714-27721.
[11] Z. Ju, G. Ma, Y. Zhao, Z. Xing, Y. Qiang, Y. Qian, *Part. Part. Syst. Char.*, 2015, **32**, 1012-1019.
[12] Z. Ju, E. Zhang, Y. Zhao, Z. Xing, Q. Zhuang, Y. Qiang, Y. Qian, *Small*, 2015, **11**, 4753-4761.
[13] N. Sivakumar, A. Narayanasamy, J. Greneche, R. Murugaraj, Y. Lee, *J. Alloys Compd.* , 2010, **504**, 395-402.
[14] C. Jia, Y. Liu, M. Schwickardi, C. Weidenthaler, B. Spliethoff, W. Schmidt, F. Schuth, *Appl. Catal., A: General.*, 2010, **386**, 94-100.
[15] Y. Liu, Z. Liu, Y. Yang, H. Yang, G. Shen, R. Yu, *Sens. Actuators, B: Chemical.*, 2005, **107**, 600-604.
[16] H. Liu, H. Liu, *J. Electron. Mater.*, 2014, **43**, 2553-2558.
[17] N. Sivakumar, S. Gnanakan, K. Karthikeyan, S. Amaresh, W. Yoon, G. Park, Y. Lee, *J. Alloys Compd.* , 2011, **509**, 7038-7041.
[18] A. Rai, T. Thi, J. Gim, J. Kim, *Mater. Charact.*, 2014, **95**, 259-265.
[19] X. Jiang, X. Zhu, X. Liu, L. Xiao, X. Ai, H. Yang, Y. Cao, *Electrochim. Acta*, 2016, **196**, 431-439.
[20] D. Du, W. Yue, X. Fan, K. Tang, X. Yang, *Electrochim. Acta*, 2016, **194**, 17-25.

[21] X. Xu, S. Chen, C. Xiao, K. Xi, C. Guo, S. Guo, S. Ding, D. Yu, R.V. Kumar, *ACS. Appl. Mater. Interfaces*, 2016, **8**, 6004-6010.
[22] B. Wang, S. Li, X. Wu, J. Liu, W. Tian, J. Chen, *New J. Chem.*, 2016, **40**, 2259-2267.
[23] C. Lei, F. Han, D. Li, W. Li, Q. Sun, X. Zhang, A. Lu, *Nanoscale*, 2013, **5**, 1168-1175.
[24] Y. Yin, B. Zhang, X. Zhang, J. Xu, S. Yang, *J. Sol-Gel Sci. Technol.*, 2013, **66**, 540-543.
[25] Y. Qi, N. Du, H. Zhang, P. Wu, D. Yang, *J. Power Sources,* 2011, **196**, 10234-10239.
[26] F. Fan, G. Fang, R. Zhang, Y. Xu, J. Zheng, D. Li, *Appl. Surf. Sci.*, 2014, **311**, 484-489.
[27] L. Yang, J. Hu, A. Dong, D. Yang, *Electrochim. Acta,* 2014, **144**, 235-242.
[28] D. Chen, W. Wei, R. Wang, J. Zhu, L. Guo, *New J. Chem.* , 2012, **36**, 1589-1595.
[29] Q. Sun, Z. Wang, Z. Zhang, Q. Yu, Y. Qu, J. Zhang, Y. Yu, B. Xiang, *ACS. Appl. Mater. Interfaces*, 2016, **8**, 6303-6308.
[30] H. Xia, Y. Wan, G. Yuan, Y. Fu, X. Wang, *J. Power Sources*, 2013, **241**, 486-493.
[31] C. Wang, L. Yin, D. Xiang, Y. Qi, *ACS. Appl. Mater. Interfaces*, 2012, **4**, 1636-1642.
[32] Y. Liu, Y. Zhan, Y. Ying, X. Peng, *New J. Chem.*, 2016, **40**, 2649-2654.
[33] Z. Zhang, Y. Wang, Q. Tan, Z. Zhong, F. Su, *J. Colloid Interface Sci.*, 2013, **398**, 185-192.
[34] H. Kim, D. Seo, H. Kim, I. Park, J. Hong, K. Park, K. Kang, *Chem. Mater.* , 2012, **24**, 720-725.
[35] Y. Cao, L. Wang, C. Feng, J. Zhang, F. Yang, S. Li, S. Jiang, Y. Liu, G. Yang, C. Zhao, F. Song, Z. Zhou, G. Yu, *Mater. Lett.*, 2014, **137**, 351-353.
[36] Q. Liu, *Electrochim. Acta,* 2014, **129**, 459-462.
[37] C. Hu, S. Guo, G. Lu, Y. Fu, J. Liu, H. Wei, X. Yan, Y. Wang, Z. Guo, *Electrochim. Acta*, 2014, **148**, 118-126.
[38] S. Gao, K. Geng, *Nano Energy*, 2014, **6**, 44-50.
[39] Y. Jiang, D. Zhang, Y. Li, T. Yuan, N. Bahlawane, C. Liang, W. Sun, Y. Lu, M. Yan, *Nano Energy*, 2014, **4**, 23-30.
[40] J. Shin, D. Samuelis, J. Maier, *Adv. Funct. Mater.*, 2011, **21**, 3464-3472.
[41] Y. Xiao, M. Cao, *ACS. Appl. Mater. Interfaces*, 2015, **7**, 12840-12849.
[42] Z. Xing, Z. Ju, J. Yang, H. Xu, Y. Qian, *Electrochim. Acta*, 2013, **102**, 51-57.
[43] Y. Yu, C. Chen, J. Shui, S. Xie, *Angew. Chem. Int. Ed.*, 2005, **44**, 7085-7089.
[44] S. Grugeon, S. Laruelle, R. Herrera-Urbina, L. Dupont, P. Poizot, J.M. Tarascon, *J. Electrochem. Soc.*, 2001, **148**, A285-A292.
[45] Y. Yu, C. Chen, Y. Shi, *Adv. Mater.*, 2007, **19**, 993-997.
[46] P. Poizot, L. Dupont, J. Tarascon, *Nature*, 2000, **407**, 496-499.
[47] H. Geng, Y. Guo, X. Ding, H. Wang, Y. Zhang, X. Wu, J. Jiang, J. Zheng, Y. Yang, H. Gu, *Nanoscale*, 2016, **8**, 7688-7694.
[48] L. Yang, G. Guo, H. Sun, X. Shen, J. Hu, A. Dong, D. Yang, *Electrochim. Acta*, 2016, **190**, 797-803.
[49] Y. Sun, X. Hu, W. Luo, F. Xia, Y. Huang, *Adv. Funct. Mater.*, 2013, **23**, 2436-2444.

Graphic abstract:

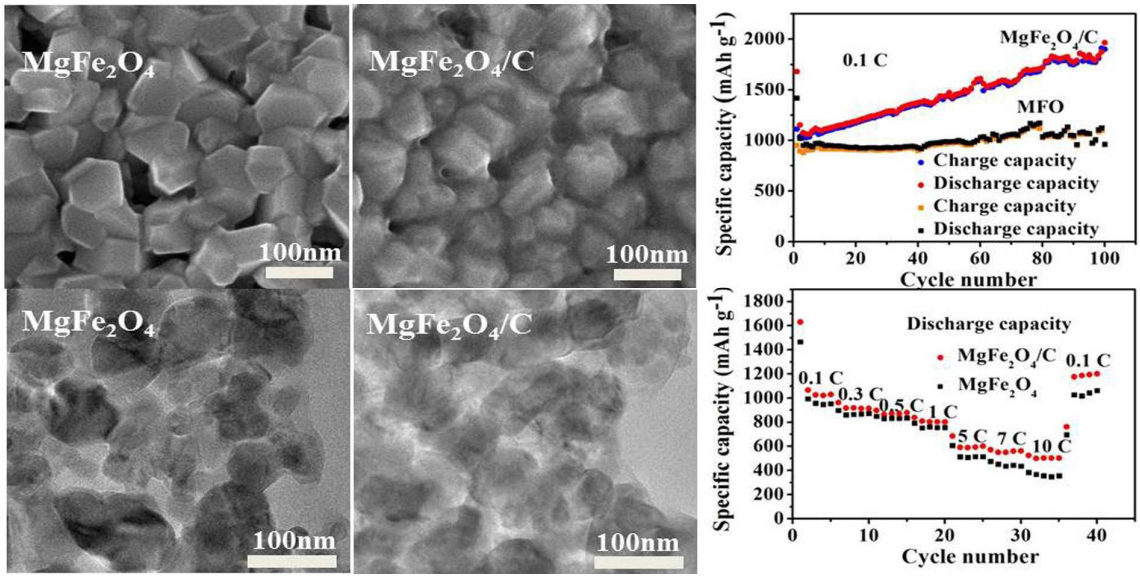

$MgFe_2O_4$/C material was synthesized via a facile method and the $MgFe_2O_4$/C electrode shows excellent cycling and rate capability.